Numerical modelling of permafrost-impacted groundwater flow systems in the context of a deep geological repository

Mahsa Malmir, John Molson & René Therrien

Department of Geology and Geological Engineering, Université Laval, Québec City, Québec, Canada

Abstract

Numerical modelling of a hypothetical geosphere setting in the Canadian Shield is employed to assess the impact of permafrost growth and decay cycles on groundwater flow and thermal conditions relevant to the near and far-field environment of a deep geological repository (DGR). This study aims to examine how transient events linked to long-term climate change and glacial cycles may affect the evolution of a deep groundwater flow system. Simplified conceptual models on relevant spatial and time scales are developed in part from field data and insights gained from a northern research site located near Umiujaq, in Nunavik, Quebec, Canada. Future climate transitions are based on the past 1 million years of air temperature data, which are considered an analogue for future changes. Simulated processes include coupled groundwater flow, heat and mass (brine) transport, with freeze/thaw, latent heat and ice-fraction dependent relative permeability. Initial simulations have shown how permafrost cycles can affect deep groundwater pathways, leading to the formation of a transient barrier that restricts groundwater flow and brine transport between the geosphere and biosphere, potentially leading to longer flow and transport pathways and increased groundwater residence times. However, the formation of below-lake taliks lakes can also maintain hydraulic connections between the geosphere and biosphere, creating transient groundwater pathways even during glacial periods. The findings of this research will provide valuable insights into the impact of future glaciations on the long-term safety of DGRs.

1 Introduction

Numerous countries, including Canada, that use nuclear power for electricity generation, are currently exploring the possibility of storing their used nuclear fuel in deep geological repositories (DGRs) located within suitable geological formations (Taylor 2021). Over the long term, some DGRs will undergo multiple glacial and climate cycles, including permafrost formation and thaw, which will significantly affect surface water hydrology networks, groundwater recharge and discharge, and deep groundwater flow systems, all of which may have implications for DGRs (Holden et al. 2009). Comprehensive studies are necessary to understand freeze-thaw cycles including permafrost during glacial periods and its impact on the long-term safety of repositories.

A large part of northern Europe and North America has been glaciated repeatedly over the past two to three million years, and such cycles are expected to continue in the future due to variations in solar insolation caused by Earth's orbital dynamics (Fischer et al. 2021). Both the ground surface and subsurface environment, including associated hydrological systems, may be affected by climate-induced changes, such as the advance and retreat of continental-scale ice sheets and permafrost. Thus, when assessing the performance of a deep geological repository, such changes must be considered (Sheppard et al. 1995; Talbot 1999).

To predict the long-term behavior of DGRs, several numerical models have been developed that consider thermal, hydraulic, mechanical, and chemical (THMC) processes. For instance, the DECOVALEX Project (Development of Coupled THMC Models and their Validation against Experiments) examined the potential impacts of glaciation on DGRs by simulating the coupled effects of THMC processes (Chan et al. 2005). Other studies, such as Walsh and Avis (2010), investigated the effects of glaciation on a hypothetical repository in the Canadian Shield, focusing on the impact of multiple glacial cycles on the long-term transport of radionuclides from a defective container, but without investigating salinity effects. Studies have also looked at the impact of long-term climatic variability on groundwater flow and permafrost dynamics in different geological settings (Scheidegger et al. 2019) as well as the impact of glaciation on groundwater flow which has been identified in northern latitudes as one of the most intense perturbations associated with long-term climate change (Chan et al. 2005).

Though much research has been conducted on permafrost modelling and groundwater flow, significant research gaps still remain regarding the significance and impact of frozen ground on the long-term stability of a repository. Areas that require further investigation include geophysical and geochemical changes induced by freezing, including pressure and hydromechanical loading, geological variability and geometrical uncertainties (Scheidegger et al. 2019), changes in groundwater flow paths, formation of taliks, groundwater salinity at depth (Scheidegger et al. 2019; Busby et al. 2015), and groundwater flow and solute transport dynamics in cold regions (Mohammed et al. 2021; McKenzie et al. 2021). Moreover, the impact of large-scale changes in permafrost over climate-cycle time scales in the context of deep flow systems and DGRs, remains poorly understood (Busby et al. 2015). Such research gaps can be filled by numerically investigating groundwater systems which include permafrost freeze/thaw and a deep zone of natural formation brines that may become perturbed over geological time.

This study aims to investigate the impact of permafrost growth and decay cycles on groundwater flow, heat, and brine transport in the near-field and far-field environments of a DGR. The analysis of cryo-hydrogeological processes will be conducted using numerical modelling coupled with

https://doi.org/10.52381/ICOP2024.83.1

field data to develop and test hypothetical conceptual models.

2 CONCEPTUAL MODEL

2.1 Geological Setting

The conceptual simulations are conducted for a hypothetical site, based in part on data from the Umiujaq permafrost research field site in Nunavik, Quebec, Canada. The approach focuses on evaluating the sensitivity of a coupled system of groundwater flow, heat and brine transport driven by surface air temperature time-series.

2.2 Surface Temperatures

Prior studies have used marine oxygen isotope ratio ($\delta^{18}O$) records to infer past temperatures (Bintanja and van de Wal 2008). In this study, a similar approach is employed, constructing the surface air temperature (SAT) using the proxy temperature record of the Northern Hemisphere (Scheidegger et al. 2019).

To account for uncertainties in past surface temperatures across the region, four different temperature scenarios spanning the last 1 million years are used (e.g., as in Scheidegger et al. (2019), with two scenarios presented here). Each scenario is generated by linearly scaling the $\delta^{18}O$ time-series. The temperature at any given time (T_t) is described using Eq. 1:

$$T_t = \frac{\delta^{18}O_t - \delta^{18}O_0}{\max(\delta^{18}O_t - \delta^{18}O_0)} \Delta T + T_0 \quad [1]$$

where T_0 is the present-day mean annual air temperature of 0.5 °C at Umiujaq, ΔT are the temperature offsets of -10, -14, -18, and -25 °C below the present temperature at the time of maximum $\delta^{18}O$ (Bintanja and van de Wal 2008; Scheidegger et al. 2019), $\delta^{18}O_t$ is the $\delta^{18}O$ value at the given time, and $\delta^{18}O_0$ is the present-day $\delta^{18}O$ value.

To predict future climate, we can draw insights from past events and assume they will repeat in the future (Busby et al. 2015; Fischer et al. 2021); here we will assume that the historic SAT will follow the same trend over the next 1 million years. Figures 1 and 2 show the global $\delta^{18}O$ time-series after Lisiecki and Raymo (2005) and the scaled surface temperature time-series in the Umiujaq region using ΔT ranging from -10 to -25 °C, respectively.

A 15,000-year spin-up cycle (Period 1 shown in Figure 2) was chosen based on test simulations to avoid artificial effects from the initial or boundary conditions. Such effects can originate, for example, from the initial permafrost or brine layers which are not in equilibrium with the boundary conditions or flow system. The present time in Figure 2 (at 15,000 yrs) is the end of period 1 (shown with the dashed black line), then the simulation continues for the next 65,000 yrs (shown as Period 2 in Figure 2, covering one glacial and interglacial period). Due to space limitations, the results are only shown for two different temperature scenarios, ΔT= -10 and -25 °C, referred to as S1 and S4 scenarios, respectively.

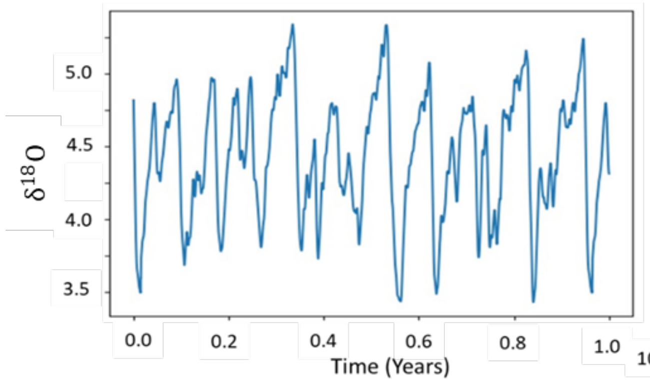

Figure 1. Global $\delta^{18}O$ time-series after Lisiecki and Raymo (2005).

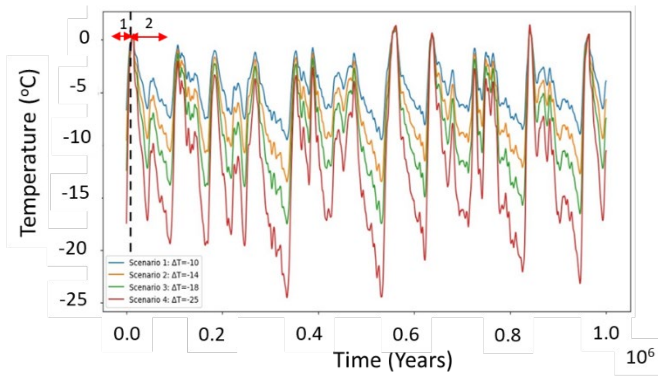

Figure 2. Scaled SAT time-series of the Umiujaq study area using ΔT ranging from -10 to -25 °C.

2.3 Numerical Model

2.3.1. Theoretical Approach

The transient groundwater flow, heat and mass transport equations were solved using the HEATFLOW-SMOKER finite element numerical model developed by Molson and Frind (2024). The model includes density-dependent groundwater flow, advective-dispersive mass transport, advective-conductive heat transport, phase change (freeze-thaw) with latent heat, and considers the influence of temperature on water density, viscosity, thermal conductivity, heat capacity, unfrozen water content, and relative permeability. Fluid density and viscosity are also concentration dependent. HEATFLOW-SMOKER has been successfully applied in many field-scale systems involving heat storage, thermal tracers, and permafrost, (e.g. Pehme et al. 2013; Shojae Ghias et al. 2018). The general advective-conductive heat transport equation, as resolved by the HEATFLOW-SMOKER code, is expressed in Eq. 2 as:

$$-\frac{\partial}{\partial x_i}\left(\theta \cdot S_w c_w \rho_w v_i T\right) + \frac{\partial}{\partial x_i}\left(\bar{\lambda} + \theta \cdot S_w c_w \rho_w D_{i,j}\right)\frac{\partial T}{\partial x_j} = \frac{\partial (C_0 T)}{\partial t} \quad [2]$$

where θ is the porosity, S_w the (unfrozen) water saturation, C_w the specific heat of water (J/kg/K), ρ_w is the water density (kg/m^3), v_i is the mean linear groundwater flow velocity (m/s), T is the temperature (°C), $\bar{\lambda}$ is the thermal conductivity of the bulk porous medium (J/m/s/K), $D_{i,j}$ the hydrodynamic dispersion coefficient (m²/s), C_o the volumetric heat capacity of the porous medium (J/m³/K), $x_{i,j}$ the spatial coordinates (m), and t is time (s). The mass transport equation can be expressed as:

$$\frac{\partial C}{\partial t} = \frac{\partial}{\partial x_i}\left(D_{i,j}\frac{\partial C}{\partial x_j}\right) - v_i\frac{\partial C}{\partial x_i} \qquad [3]$$

where C is the concentration. Picard iteration is applied to handle all nonlinearities (Molson and Frind, 2022). Expressions for the unfrozen water saturation function (W_u) and relative permeability (k_r) are given in Eqs. 4, 5, and 6, respectively:

$$W_u(T) = p + (1-p)\cdot e^{(q\cdot T)} \quad \text{for } T < 0°\mathrm{C} \qquad [4]$$

$$W_u(T) = 1 \quad \text{for } T \geq 0°\mathrm{C} \qquad [5]$$

$$k_r = \max\left[10^{-\Omega\cdot\theta(1-w_u(T))}, 10^{-6}\right] \qquad [6]$$

where p is the terminal fraction of unfrozen moisture at a very low temperature, q is a corresponding shape factor, and Ω is an empirical impedance factor. All parameters, including the thermal properties for the solids, water, and ice fractions, are presented in Table 1. For simplicity and due to the absence of site-specific data, the freezing function parameters p, q, and Ω were assumed uniform throughout the domain, consistent with the chosen geological settings. Furthermore, the relative permeability function described by Eq. 6 varies with the porosity of each unit (see Table 2). Units with higher porosity have a steeper decrease in relative permeability as the temperature decreases.

Table 1. Model parameters.

Properties and parameters	Value
Density of water (ρ_w; reference at 4 °C)	1,000 kg/m³
Density of ice (ρ_i)	920 kg/m³
Thermal conductivity of water (λ_w)	0.58 W/m K
Thermal conductivity of ice (λ_i)	2.14 W/m K
Specific heat of water (c_w)	4,187 J/kg K
Specific heat of ice (c_i)	2,108 J/kg K
Latent heat of water (L)	3.34×10^5 J/kg
Terminal unfrozen water saturation (p)*	0.01
Shape factor for unfrozen water saturation (q)*	1.0
Impedance factor (Ω) for k_r (Eq. 6)	10

* See Eqs. 4 and 5

2.4. Model Domain and Physical Properties

The 2D conceptual model is 5000 m long and 500 m deep, discretized using 500 × 50 (= 25,000) elements in the horizontal and vertical directions, respectively (Figure 3). The model consists of three hydro-stratigraphic layers, including a shallow aquifer underlain by two progressively less permeable hydrogeological units, with an initial 4.5 km long permafrost layer. The thermal and hydraulic properties of these layers are provided in Table 2. The permafrost extends between 290 m and 490 m elevation. Two lakes (Lake 1 and Lake 2) are also included within the model domain.

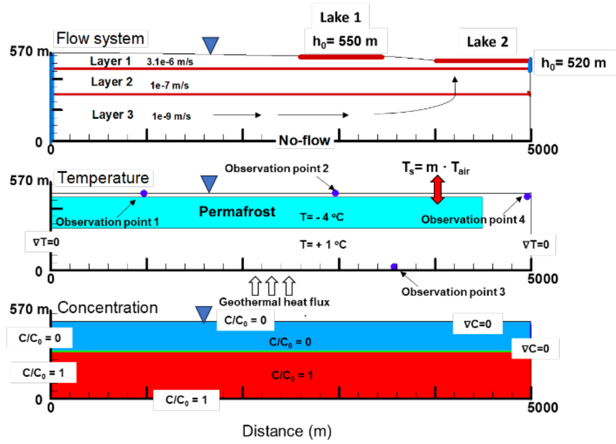

Figure 3. Boundary and initial conditions for flow, heat, and mass transport processes.

Table 2. Thermal and hydraulic properties assumed for the hydro-stratigraphic layers (Lemieux et al. 2020; Dagenais et al. 2020).

Layer	K* (ms^{-1})	θ (-)	λ_s (J/m/s/K)	c_s (J/kg/K)	ρ_s (kg/m³)
Layer 1	3.1×10^{-6}	0.120	3.0	850	2650
Layer 2	10^{-7}	0.075	2.8	850	2650
Layer 3	10^{-9}	0.001	2.0	850	2650

*K: Hydraulic conductivity

2.5 Boundary and Initial Conditions

2.5.1 Groundwater Flow System

The flow system is driven by a fixed watertable represented by two quarter-cosine functions separated by Lake 1, which is assigned a constant head of 550 m (Figure 3). Further downgradient, Lake 2 assumes the role of the main discharge zone, situated at the far right of the top boundary with a head of 520 m. Although a fixed Type-1 watertable is usually not recommended in most flow models due to its tendency to overly restrict solutions and potentially lead to unrealistic recharge rates, it can be beneficial under freeze-thaw conditions since the recharge rate adapts automatically depending on the freeze-thaw state of the shallow groundwater. The base boundary is set as no-flow (impermeable), the left boundary is assigned a fixed head of 570 m, and the upper part of the right boundary was assigned a head of 520 m. This adherence to the maximum watertable elevation at the left boundary enables inflow (when thawed) from an upgradient area beyond the model domain, progressing toward the discharge zone. Four observation points (P1, P2, P3, and P4; Figure 3), are also included, allowing the computed heads, temperatures, and concentrations to be tracked over time.

2.5.2 Heat Transport System

The left and right thermal boundaries are characterized by zero-gradient temperature conditions, implying negligible horizontal conductive heat transport (Figure 3). Following the approach used by Liu et al. (2022), the top boundary is assigned transient Type-1 (Dirichlet) temperatures determined from regressed linear relationships (m-factors) between surface air temperatures (SATs) and ground temperatures observed at Salluit, a research station north of Umiujaq. For each of two surface classes, being plateau and lakes, a freezing and thawing slope (m_f and m_t) is assigned. Here, the plateau (upgradient and inter-lake area) m-factors are assumed the same, defined by $m_f = m_t = 0.8$ for the freezing and thawing domains, respectively, while for the two lakes we assume $m_f = 0.04$ and $m_t = 0.8$, respectively. The model base is assigned a geothermal heat flux of 0.05 W/m² (Ling and Zhang 2004). The initial permafrost temperature is set at -4 °C, while the rest of the domain is initially set to +1 °C.

2.5.3 Mass Transport System

For mass transport, a fixed relative concentration of C/Co = 0 is applied at watertable recharge areas and along the upper part of the left boundary to represent freshwater infiltration. Zero-gradient conditions are imposed on discharge boundaries, including those along discharge zones of Lake 1 and 2, allowing advective discharge of fresh or salt water. A normalized concentration of C/Co = 1, corresponding to a brine total dissolved solids (TDS) concentration of 34,500 mg/L, is imposed along the bottom boundary and as the initial condition below the permafrost, extending from 0 to 300 m in elevation, whereas C/Co = 0 is applied as the initial condition in the rest of the system.

3 SIMULATION RESULTS

Simulation results of the two temperature scenarios are presented in Figure 4 a, b, c, and d (base Scenario S1) and in Figure 5 a, b, c, and d (colder Scenario S4) at 5k, 20k, 50k, and 80k yrs, showing simulated hydraulic heads and streamtraces (particle tracks), temperatures, TDS concentrations as well as hydraulic conductivity.

3.1 Flow System

The simulated flow systems clearly indicate the presence of distinct recharge and discharge zones, with noticeable variations in flow rates due to geological structure and permafrost (Figures 4a and 5a). Groundwater originates from upgradient regions at the left and flows towards the lake discharge areas. In these conceptual models, Lake 2 serves as a discharge zone, while Lake 1 plays a dual role, functioning as both a recharge zone and a discharge zone. Groundwater flow is slower in areas of permafrost, indicated by dense time markers, while flow is faster below the permafrost and within the warmer taliks below the two lakes (e... Figures 4a at 80k yrs and 5a at 50k and 80k yrs).

An important distinction emerges between the two scenarios S1 (warmer SAT) and S4 (colder SAT), with generally lower flow velocities in S4 due to more extensive freezing of the system where conductive heat transport dominates. As shown in Figure 4 a and b in the warmer S1 SAT scenario, while groundwater tends to follow paths of least resistance in thawed zones, it can also pass through the permafrost layers. At 80k yrs, for example (Figure 4a), although the system is frozen down to an elevation of approximately 250 m (indicated by the 0 °C isotherm), some groundwater entering from the left boundary below the permafrost still tends to flow through the permafrost towards the discharge zones. Note that because of the assumed freezing function for k_r (Eq 4), flow velocities do not abruptly decrease at the freezing front, but decrease exponentially until temperatures decrease to about -3 or -4 °C. Although velocities are much lower within the permafrost, they can still be significant on geological time scales (depending also on the intrinsic unfrozen K).

Advective particle tracks (superimposed on the hydraulic head fields in Figures 4a and 5a) are used to estimate advective travel times through the flow system. Since they are generated assuming a steady-state flow system at specific times, the particle tracks are not meant to be representative of radionuclide transport from a potential DGR. In both scenarios, travel times extend to millions of years which is much longer than the estimated lifespan of a DGR (Taylor 2021). However, as they represent only snapshots of the transient system, these travel times are likely overestimated during peak glaciation and underestimated during interglacial periods.

3.2 Heat Transport System

The temperature distributions and permafrost depths for both scenarios, represented by the 0 °C isotherm, are shown in Figures 4b and 5b. Only Scenario S4 (colder SAT) produces a permafrost depth reaching the reference depth associated with an assumed DGR 500 m deep. The thermal regime shows a generally stratified system due to strong thermal conduction, with the T = 0 °C isotherm propagating deeper over time following the 15k-yr warming spin-up period. (Note, the SATs for each scenario are provided in Figure 2 and in more detail in Figure 6a).

At 5,000 yrs in each scenario (Figures 4b and 5b), the system is still in a warming phase starting from the assumed initial condition with the extensive permafrost layer. At 20k yrs, the two systems are near their warmest, being only 5k yrs after the peak SATs (Figure 6a). Domain temperatures from 20k to 80k yrs are generally cooling, despite the short warming trend in the SAT from about 45k to 55k yrs. Because of thermal insulation of the lakes, warmer zones persist below each lake in the form of taliks.

The results also highlight the influence of the underlying thermal state on groundwater flow, including the effect on groundwater discharge to Lake 1 and Lake 2. As an example, in the warmer Scenario S1 and the colder Scenario S4, Figures 4a, b and 5a, b show that despite the freezing conditions beneath the plateau (upgradient) areas, Lakes 1 and 2 continue to serve as discharge zones.

3.3 Mass Transport System

Changes in long-term surface temperature conditions also lead to variations in the position and characteristics of the brine interface. The simulated interface is affected by the transient flow system which depends on the concentration-dependent fluid density and viscosity, as well as on the temperature-dependent relative permeability (through the variable ice content). This coupling between temperature conditions and flow dynamics highlights the sensitivity of the brine system to climatic variations. Nevertheless, except for the below-lake talik regions, the generally lower hydraulic conductivities at depth upgradient of the lakes due to both geologic structure and lower ice-fraction dependent relative permeabilities result in limited changes to the depth and movement of the brine interface.

Despite the high density of the brine, which tends to stabilize the interface, the gravity-induced groundwater flow system depresses the brine interface between through the warmer and thus more permeable taliks, where flow is diverted deeper below the inter-lake frozen zone (Figure 4b, c and 5b, c at 50k and 80k yrs). Initial stages of the S1 simulation show a dynamic system of infiltrating fresh water, leading to brine dilution beneath Lake 1 (Figure 4c). As the system warms during the 15k yr spin-up, by 20k yrs, the initial cold front between the two taliks has significantly thawed, and brine migrates upward toward the Lake 2 discharge zone. At 50k yrs, as the system cools, the downward extension of the cold front below the inter-lake area forces infiltrating upgradient freshwater to circumvent the inter-lake frozen zone and pass through the thawed and thus higher permeability layers, pushing down the brine interface. This behavior intensifies at 80k yrs when the system becomes even colder. A similar pattern can be seen with a greater impact in the colder Scenario S4 (Figure 5c).

3.4 Hydraulic Conductivities

Effective hydraulic conductivities reflect variability in both the imposed geological structure and the transient freeze/thaw state (Figure 4d and 5d). While some geological structure is still evident at early time as horizontal stratification (at 5k and 20k yrs), by 50k and 80k yrs the impact of ice-fraction dependent relative permeability becomes significant as the system freezes and lateral changes in hydraulic conductivity due to the below-lake taliks become more apparent. Specifically, in the upgradient (left) half of the domain between 400 and 450-m elevations, the temperature-dependent hydraulic conductivity is lower compared to the areas within the warmer taliks below each lake (Figure 4b, d). Groundwater velocities are thus also significantly lower compared to other parts of the domain (Figure 4a). Similar behavior can also be observed in Figure 5b, d, for the colder Scenario S4.

3.5 Breakthrough Curves

Breakthrough (arrival) curves for temperature and concentration are provided in Figure 6a and b, respectively, at monitor points P1–P4; the input SATs are also included in Figure 6a. Note that in both scenarios, a SAT temperature peak occurs at around 15k yrs (the assumed present time) and a temperature dip occurs around 45k yrs, followed by a rapid rise and a clear peak shortly around 55k yrs. Directly beneath Lake 1 (at P2), the temperatures for both scenarios remain near 0 °C because of the imposed freezing m-factors of m_f = 0.04 (Figure 6a). At the deeper point P3, the minimum and maximum temperatures align with the SAT in both scenarios but are also influenced by the geothermal flux at the model base, contributing to warmer temperatures. In warmer Scenario S1, characterized by higher flow velocities and a more dynamic environment compared to S4, upward migration of brine to P4 at Lake 2 occurs somewhat faster compared to Scenario S4, especially after 40k yrs (Figure 6b). In both scenarios, over geological time, the flow system tends to induce continued upward migration of the brine towards Lake 2, despite the cooling temperatures. This is accentuated in the warmer scenario S1 with a more dynamic system. In both scenarios, the relatively small and short-lived SAT temperature peak at around 55k yrs has no significant impact on salt transport toward the discharge zone (Figure 6b).

4. Discussion

The simulations have demonstrated the influence of geological structure and climate-induced freeze-thaw processes on deep regional groundwater flow systems. Although the presence of permafrost decreases the effective hydraulic conductivity of the host rock, under the assumed conditions of a non-zero unfrozen water content at low temperature, groundwater flow through permafrost (i.e., 80k yrs in S1 and 50k and 80k yrs in S4) can still be significant over glacial/interglacial time scales depending on the relative permeability and hydraulic gradients.

The presence of taliks beneath lakes can establish a deep link between the geosphere and biosphere, generating transient groundwater pathways even during glacial conditions. The study also highlighted the sensitivity of the system to climatic variations and the influence of subsurface permeability on brine transport dynamics. Subsurface temperatures need to decrease to at least -3 to -4 °C before the flow velocities are significantly reduced. In both scenarios, the salt concentration steadily increases in the discharge area of Lake 2 with a more pronounced effect in warmer Scenario S1 due to higher flow velocities compared to S4.

In these scenarios, because of the relatively low temperature variations, the effect of concentration-dependent fluid density is more significant than the impact of temperature-dependent density. The simulated temperature trends at the screening points follow the SAT trends, with more influence in deeper layers from the geothermal flux in deeper layers. Furthermore, comparing times of glacial maximum conditions and corresponding temperatures underscores the dynamic relationship between Surface Air Temperature (SAT) and the subsurface flow system's response time. This aspect highlights the system's complex behavior under varying thermal conditions.

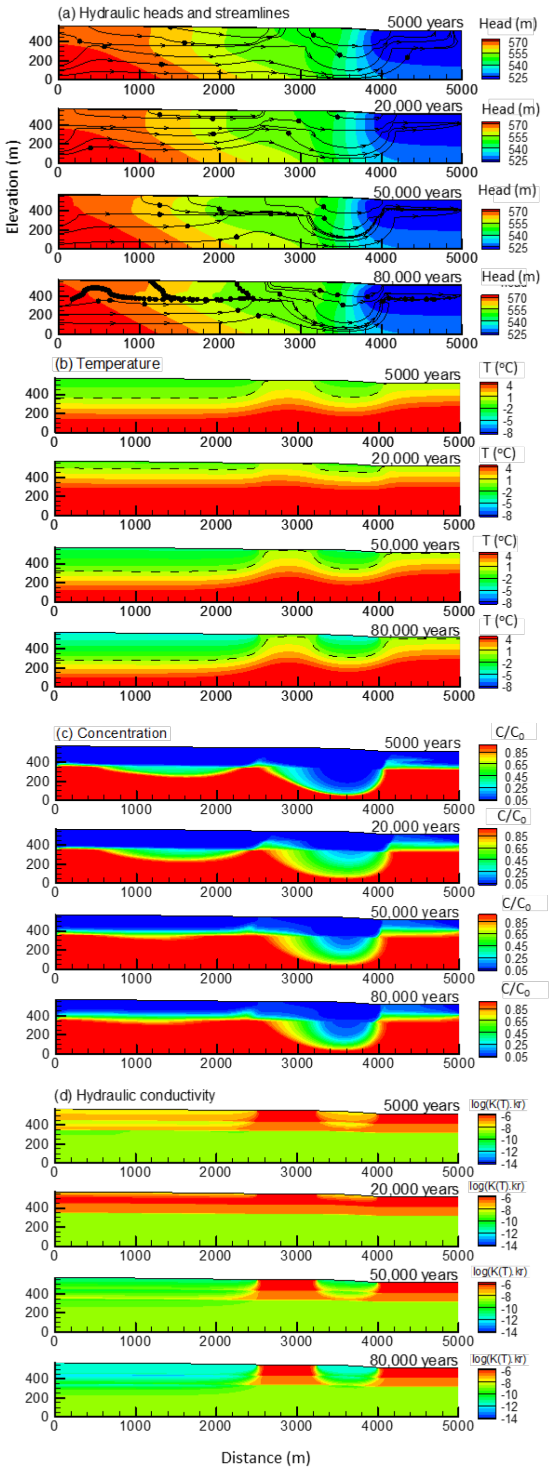

Figure 4. Simulated results over time, Scenario S1 (warmer): (a) hydraulic heads and particle tracks (time marker interval is 80k yrs.), (b) temperature, (c) concentration and (d) hydraulic conductivity. C/Co = 1 corresponds to 34,500 mg/L TDS.

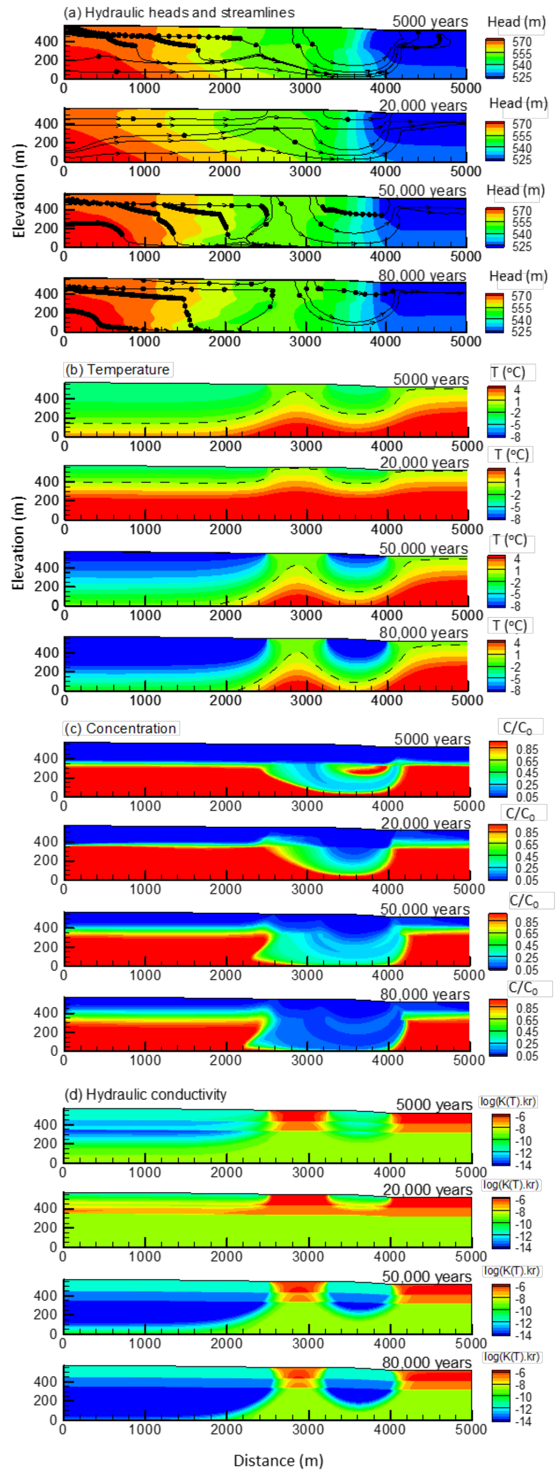

Figure 5. Simulated results over time, Scenario S4 (colder): (a) hydraulic heads and particle tracks (time marker interval is 800k yrs.), (b) temperature, (c) concentration and (d) hydraulic conductivity. C/Co = 1 corresponds to 34,500 mg/L TDS.

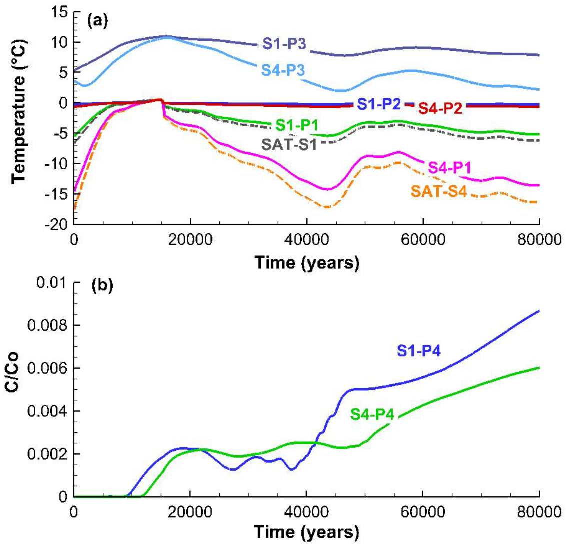

Figure 6. Simulated breakthrough curves at selected observation points for Scenarios S1 and S4, showing: (a) temperature and (b) concentrations; C/Co = 1 corresponds to 34,500 mg/L TDS. Dashed lines in (a) are surface air temperatures (SATs) for Scenarios S1 and S4.

The long travel times underscore the enduring effects of past glacial periods on subsurface hydrodynamics. This highlights the importance of considering paleoclimatic conditions in understanding present-day subsurface flow patterns.

The results emphasize the need to consider climatic conditions, geological structure, and freeze-thaw processes when evaluating the suitability of a potential DGR site. Insights have been provided into the behavior of deep cryo-hydrogeological systems and the importance of improving our understanding of groundwater flow, heat transport, and solute transport dynamics in cold regions.

5 Model Limitations and Future Work

Several limitations and assumptions must be recognized while interpreting the results. Groundwater flow was assumed fully saturated, and cryo-suction, ice segregation, and effects of glacial loading and unloading were neglected. Ice-fraction dependent unfrozen moisture content and relative permeability are only temperature dependent and neglect effects of salt concentration. Furthermore, the adopted continuum approach assumes a fully connected pore space, in particular for the terminal unfrozen moisture content. Longer simulations including warmer and colder periods over multiple glacial cycles should be carried out. Future studies should also conduct sensitivity analyses of hydraulic properties to understand performance under different geological and climatic conditions, with particular focus on the impact of the unfrozen moisture content (freezing function).

6 Summary and Conclusions

In this study we have used numerical simulations to investigate the potential impact of permafrost growth and decay cycles on groundwater flow, heat, and brine transport in the context of a DGR. The conceptual model was designed to incorporate key processes of density-dependent groundwater flow, advective-conductive heat transport, and advective-dispersive mass (brine) transport, including water-ice phase change, and latent heat effects. The findings enhance our understanding of the coupling between groundwater flow, heat transport, and brine transport in permafrost environments.

In addition, the study emphasized the system's sensitivity to climatic fluctuations and the role of subsurface permeability in brine transport dynamics, while also shedding light on how temperature variations impact groundwater flow rates and patterns, specifically in relation to groundwater discharge into surface water bodies.

The study also highlights the pivotal role of unfrozen moisture content in allowing groundwater flow through parts of the frozen ground that still contain liquid water, suggesting that unfrozen water within permafrost can control groundwater flow behavior. More investigation on defining realistic values of unfrozen moisture content and their effect on such systems seems to be necessary.

The system's behavior is complex under varying surface temperatures and density-dependent thermohaline conditions. Although only relatively low salt concentrations were assumed here (on the order of seawater), on these geological time scales changes in fluid density due to salt content still played a significant role in affecting the flow field. Effects of salt concentrations on density were clearly more significant than those of temperature.

7 Acknowledgements

The authors thank the NWMO (Nuclear Waste Management Organization Canada) for funding this research project. Additionally, we acknowledge the support of the CatchNet research group (https://skb.se/catchnet/this-is-catchnet/). Special thanks are also extended to the CEN (Centre d'études nordiques) and CentrEau (Centre de recherche sur l'eau) for their contributions and support.

8 References

Bintanja, R. and van de Wal, R. 2008. ‘North American ice-sheet dynamics and the onset of 100,000-year glacial cycles’, *Nature* 454, pp. 869–872.

Busby, J., Lee, J., Kender, S., Williamson, J., and Norris, S. 2015. ‘Modelling the potential for permafrost development on a radioactive waste geological disposal facility in Great Britain’, *Proceedings of the Geologists’ Association* 126 (2015), pp. 664–674. Available at: https://doi.org/10.1016/j.pgeola.2015.06.001.

Chan, T., Christiansson, R., Boulton, G., Ericsson, L., Hartikainen, J., Jensen, M., Ivars, D.M., Stanchell, F., Vistrand, P., and Wallroth, T. 2005. 'DECOVALEX III BMT3/BENCHPAR WP4: The thermo-hydromechanical responses to a glacial cycle and their potential implications for deep geological disposal of nuclear fuel waste in a fractured crystalline rock mass', *International Journal of Rock Mechanics and Mining Sciences* 42, pp. 805–827.

Dagenais, S., Molson, J., Lemieux, J.-M., Fortier, R., and Therrien, R. 2020. 'Coupled cryo-hydrogeological modelling of permafrost dynamics near Umiujaq (Nunavik, Canada)', *Hydrogeology Journal* 28, pp. 887–904.

Fischer, U.H., Bebiolka, A., Brandefelt, J., Cohen, D., Harper, J., Hirschorn, S., Jensen, M., Kennell, L., Liakka, J., Näslund, J.-O., et al. 2021. 'Radioactive waste under conditions of future ice ages', in W. Haeberli and C. Whiteman (eds.), *Snow and Ice-Related Hazards, Risks, and Disasters (Second Edition)*. Amsterdam, Netherlands: Elsevier.

Holden, B., Stotler, R., Frape, S., Ruskeeniemi, T., Talikka, M., and Freifeld, B.M. 2009. 'High lake permafrost comparison site: permafrost phase IV', *Nuclear Waste Management Organization* NWMO TR-2009-11.

Lemieux, J-M., Fortier, R., Murray, R., Dagenais, S., Cochand, M., Delottier, H., Therrien, R., Molson, J., Pryet, A., and Parhizkar, M. 2020. 'Groundwater dynamics within a watershed in the discontinuous permafrost zone near Umiujaq (Nunavik, Canada)', *Hydrogeology Journal* 28(3), pp. 833–851.

Ling, F. and Zhang, T. 2004. 'A numerical model for surface energy balance and thermal regime of the active layer and permafrost containing unfrozen water', *Cold Regions Science and Technology* 38(1), pp. 1–15.

Lisiecki, L.E. and Raymo, M.E. 2005. 'A Pliocene-Pleistocene stack of 57 globally distributed benthic δ18O records', *Paleoceanography* 20(1).

Liu, W., Fortier, R., Molson, J., Lemieux, J.M. 2022. 'Three-dimensional numerical modeling of cryo-hydrogeological processes in a river-talik system in a continuous permafrost environment', *Water Resources Research* 58(3), 2021WR031630.

McKenzie, J.M., Kurylyk, B.L., Walvoord, M.A., Bense, V.F., Fortier, D., Spence, C., and Grenier, C. 2021. 'Invited perspective: What lies beneath a changing Arctic?', *The Cryosphere* 15, pp. 479–484.

Mohammed, A.A., Bense, V.F., Kurylyk, B.L., Jamieson, R.C., Johnston, L.H., and Jackson, A.J. 2021. 'Modeling reactive solute transport in permafrost-affected groundwater systems', *Water Resources Research* 57, e2020WR028771.

Molson, J.W. and Frind, E.O. 2024. *HEATFLOW-SMOKER USER GUIDE, Density-dependent flow and advective-dispersive transport of mass, thermal energy or residence time in 3D fractured porous media, Version 5.0*. Université Laval and University of Waterloo.

Pehme, P., Parker, BL., Cherry, J.A., Molson, J.W., and Greenhouse, J.P. 2013 'Enhanced detection of hydraulically active fractures by temperature profiling in lined heated bedrock boreholes', *Journal of Hydrology* 484, pp.1–15.

Scheidegger, J.M., Jackson, C.R., McEvoy, F.M. and Norris, S. 2019. 'Modelling permafrost thickness in Great Britain over glacial cycles', *Science of the Total Environment* 666, pp. 928–943

Sheppard, M.I., Amiro, B., Davis, P., and Zach, R. 1995. 'Continental glaciation and nuclear fuel waste disposal: Canada's approach and assessment of the impact on nuclide transport through the biosphere', *Ecological modelling* 78, pp. 249–265.

Shojae Ghias, M., Therrien, R., Molson, J., and Lemieux, J-M. 2018. 'Numerical simulations of shallow groundwater flow and heat transport in a continuous permafrost setting under the impact of climate warming', *Canadian Geotechnical Journal*, 56(3), pp. 436–448.

Talbot, C. 1999. 'Ice ages and nuclear waste isolation', *Engineering Geology* 52, pp. 177–192.

Taylor, A. 2021. 'Deep Geological Repository Transportation System Conceptual Design Report Crystalline/Sedimentary Rock, Technical Report', *Nuclear Waste Management Organization*, APMREP-00440-0209-R001.

Walsh, R. and Avis, J., 2010. 'Glaciation Scenario: Groundwater and Radionuclide Transport Studies, Technical Report', *Nuclear Waste Management Organization* (NWMO) DGR TR-2010-09.